

---

---

# In Vivo Quantification of ER $\beta$ Expression by Pharmacokinetic Modeling: Studies with $^{18}\text{F}$ -FHNP PET

Inês F. Antunes<sup>1</sup>, Antoon T.M. Willemsen<sup>1</sup>, Jurgen W.A. Sijbesma<sup>1</sup>, Ate S. Boerema<sup>1,3</sup>, Aren van Waarde<sup>1</sup>, Andor W.J.M. Glaudemans<sup>1</sup>, Rudi A.J.O. Dierckx<sup>1</sup>, Elisabeth G.E. de Vries<sup>2</sup>, Geke A.P. Hospers<sup>2</sup>, and Erik F.J. de Vries<sup>1</sup>

<sup>1</sup>Department of Nuclear Medicine and Molecular Imaging, University Medical Center Groningen, University of Groningen, Groningen, The Netherlands; <sup>2</sup>Department of Medical Oncology, University Medical Center Groningen, University of Groningen, Groningen, The Netherlands; and <sup>3</sup>Groningen Institute for Evolutionary Life Sciences, University of Groningen, Groningen, The Netherlands

---

The estrogen receptor (ER) is a target for endocrine therapy in breast cancer patients. Individual quantification of ER $\alpha$  and ER $\beta$  expression, rather than total ER levels, might enable better prediction of the response to treatment. We recently developed the tracer 2- $^{18}\text{F}$ -fluoro-6-(6-hydroxynaphthalen-2-yl)pyridin-3-ol ( $^{18}\text{F}$ -FHNP) for assessment of ER $\beta$  levels with PET. In the current study, we investigated several pharmacokinetic analysis methods to quantify changes in ER $\beta$  availability with  $^{18}\text{F}$ -FHNP PET. **Methods:** Male nude rats were subcutaneously inoculated in the shoulder with ER $\alpha$ /ER $\beta$ -expressing SKOV3 human ovarian cancer cells. Two weeks after tumor inoculation, a dynamic  $^{18}\text{F}$ -FHNP PET scan with arterial blood sampling was acquired from rats treated with vehicle or various concentrations of estradiol (nonspecific ER agonist) or genistein (ER $\beta$ -selective agonist). Different pharmacokinetic models were applied to quantify ER $\beta$  availability in the tumor. **Results:** Irreversible-uptake compartmental models fitted the kinetics of  $^{18}\text{F}$ -FHNP uptake better than reversible models. The irreversible 3-tissue-compartment model, which included both the parent and the metabolite input function, gave results comparable to those of the irreversible 2-tissue-compartment model with only a parent input function, indicating that radioactive metabolites contributed little to the tumor uptake. Patlak graphical analysis gave metabolic rates ( $K_i$ , the irreversible uptake rate constant) comparable to compartment modeling. The  $K_i$  values correlated well with ER $\beta$  expression but not with ER $\alpha$ , confirming that  $K_i$  is a suitable parameter to quantify ER $\beta$  expression. SUVs at 60 min after tracer injection also correlated ( $r^2 = 0.47$ ;  $P = 0.04$ ) with ER $\beta$  expression. A reduction in  $^{18}\text{F}$ -FHNP tumor uptake and  $K_i$  values was observed in the presence of estradiol or genistein. **Conclusion:**  $^{18}\text{F}$ -FHNP PET enables assessment of ER $\beta$  availability in tumor-bearing rats. The most suitable parameter to quantify ER $\beta$  expression is the  $K_i$ . However, a simplified static imaging protocol for determining the SUVs can be applied to assess ER $\beta$  levels.

**Key Words:** estrogen receptors; pharmacokinetics; PET; quantification; oncology

**J Nucl Med 2017; 58:1743–1748**

DOI: 10.2967/jnumed.117.192666

**T**he estrogen receptor (ER), which is involved in the development and progression of hormone-sensitive cancers, operates as a ligand-dependent transcription factor that modulates oncogenesis and inhibits tumor suppressor genes. ER is a key target in endocrine therapies, aiming to inhibit hormone signaling in hormone-sensitive cancers (1), and consists of 2 isoforms—ER $\alpha$  and ER $\beta$ —which have opposite physiologic effects. Activation of ER $\alpha$  by estrogens induces cell proliferation and cell survival, whereas activation of ER $\beta$  leads to the formation of a heterodimer ER $\alpha$ –ER $\beta$  complex that inhibits ER $\alpha$  signaling and promotes apoptosis (2). Expression of ER $\beta$  was suggested to be an independent predictive marker for benefit from tamoxifen treatment in patients with ER $\alpha$ -negative breast tumors, in which tamoxifen treatment is usually considered to be ineffective (3).

Currently, the primary surgical specimen or a tumor biopsy is used to assess ER tumor status. However, receptor expression in the tumor can change over time. Crosstalk of ER with growth factor receptors can also lead to changes in ER expression (4,5). Since ER $\alpha$  and ER $\beta$  can induce opposite effects and ER status can convert over time, either spontaneously or induced by treatment, a suitable tool to determine ER phenotypes of all lesions in a patient would be of great importance. Currently, 17 $\beta$ - $^{18}\text{F}$ -fluoro-16 $\alpha$ -estradiol (FES) is used as a PET tracer for assessment of the ER status of breast cancer metastases. ER imaging can have an important impact on patient management, as  $^{18}\text{F}$ -FES PET was shown to be responsible for a change in the intended treatment in a high percentage of patients presenting with a diagnostic dilemma (6). However,  $^{18}\text{F}$ -FES has poor subtype selectivity and therefore does not provide information about the ER subtype. Subtype-selective PET tracers would enable better characterization of tumor lesions and, therefore, better assessment of their sensitivity toward endocrine therapies. ER $\beta$ -selective tracers might also be of interest for assessment of ER $\beta$  in lung carcinomas and lung fibrosis (7,8). Furthermore, imaging of ER subtypes may provide more insight into the mechanisms of resistance to hormonal treatment and crosstalk of ER with other signaling pathways.

Recently, we developed the PET tracer 2- $^{18}\text{F}$ -fluoro-6-(6-hydroxynaphthalen-2-yl)pyridin-3-ol ( $^{18}\text{F}$ -FHNP), which selectively binds to ER $\beta$  (9). However,  $^{18}\text{F}$ -FHNP uptake in tumors has been relatively low compared with  $^{18}\text{F}$ -FES uptake. Possible explanations for the observed low tumor uptake are low ER $\beta$  expression in the tumor and low influx ( $K_i$ ) due to poor perfusion or rapid metabolism of the tracer. To discriminate between these possible explanations, we further analyzed the metabolism of

---

Received Mar. 16, 2017; revision accepted May 26, 2017.

For correspondence or reprints contact: Inês F. Antunes, Department of Nuclear Medicine and Molecular Imaging, University Medical Center Groningen, University of Groningen, P.O. Box 30.001, 9700 RB Groningen, The Netherlands.

E-mail: i.farinha.antunes@umcg.nl.

Published online Jul. 13, 2017.

COPYRIGHT © 2017 by the Society of Nuclear Medicine and Molecular Imaging.

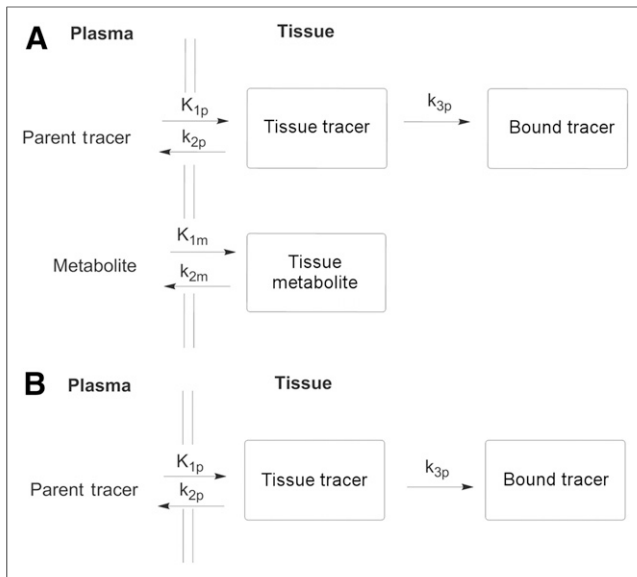


**FIGURE 1.** Compartmental models applied for  $^{18}\text{F}$ -FHNP kinetic analysis: irreversible 3TCM (A) and irreversible 2TCM (B).  $K_{1p}$  = uptake constant of intact parent (mL/g/min);  $k_{2p}$  = clearance rate of intact parent (1/min);  $k_{3p}$  = selective binding of intact parent (1/min);  $K_{1m}$  = uptake constant of metabolites (mL/g/min);  $k_{2m}$  = clearance rate of metabolites (1/min).

$^{18}\text{F}$ -FHNP and its pharmacokinetics in tumor-bearing rats. To assess the validity of  $^{18}\text{F}$ -FHNP PET for imaging of ER $\beta$  expression, several imaging parameters were correlated with the ER $\beta$  expression levels, as determined by Western blotting.

## MATERIALS AND METHODS

### Synthesis of $^{18}\text{F}$ -FHNP

$^{18}\text{F}$ -FHNP was prepared as previously described (9).  $^{18}\text{F}$ -FHNP was obtained within 115 min in  $9\% \pm 4\%$  radiochemical yield (decay-corrected, based on  $^{18}\text{F}$ -fluoride). Quality control was performed by ultra-performance liquid chromatography, using an HSS-T3 column (1.8  $\mu\text{m}$ ,  $3.0 \times 50$  mm; Waters) with 30% aqueous acetonitrile as the mobile phase at a flow of 1 mL/min. At the end of synthesis, the molar activity was  $378 \pm 84$  GBq/ $\mu\text{mol}$  and the radiochemical purity was always greater than 98%.

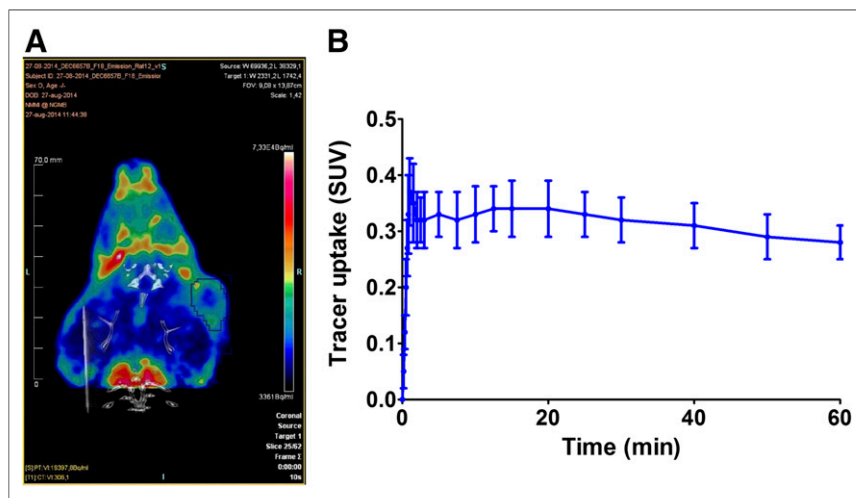


**FIGURE 2.** (A) Coronal small-animal PET/CT fusion images of rat bearing SKOV3 xenograft injected with  $^{18}\text{F}$ -FHNP (21.5 MBq). (B) Averaged time-activity curve of  $^{18}\text{F}$ -FHNP uptake in SKOV3 xenografts ( $n = 9$ ).

## Animals

Male nude rats were obtained from Harlan ( $n = 32$ ). The animals were provided with standard laboratory chow and tap water ad libitum. All studies were performed in compliance with Dutch law and the local ethical guidelines for animal experiments. The protocol was approved by the Institutional Animal Care and Use Committee (DEC 6657B). After the rats had been acclimatized for at least 1 wk, SKOV3 cancer cells ( $10^6$  cells in a 1:1 mixture of Matrigel and Dulbecco modified Eagle medium [high-glucose] with 10% fetal bovine serum) were subcutaneously injected into the upper back of the rats. Approximately 15 d after inoculation, palpable tumor nodules were formed. The animals were randomly divided into different groups: control animals ( $n = 9$ ), animals administered different concentrations of the nonspecific ER agonist estradiol ( $n = 14$ ), and animals administered the ER $\beta$ -specific agonist genistein ( $n = 9$ ).

## PET Imaging

Two weeks after tumor inoculation, a 60-min dynamic PET scan with arterial blood sampling was obtained. The animals were anesthetized with isoflurane (5% for induction and 2% for maintenance), a cannula was inserted in the femoral artery for blood sampling, and a second cannula was inserted in the femoral vein for tracer injection. The animals were carefully positioned in the PET camera (microPET Focus 220; Siemens) with their tumors in the center of the field of view. A transmission scan of 515 s with a  $^{57}\text{Co}$  point source was obtained for correction of attenuation and scatter. A mixture of  $^{18}\text{F}$ -FHNP ( $15.7 \pm 4.6$  MBq, 1 mL) with estradiol (0.3  $\mu\text{g/g}$  [ $n = 4$ ], 0.03  $\mu\text{g/g}$  [ $n = 5$ ], 0.003  $\mu\text{g/g}$  [ $n = 5$ ]) in phosphate-buffered saline or vehicle ( $n = 5$ ) was injected via the femoral vein using an injection pump set at a flow rate of 1 mL/min. In another group of animals, genistein (5  $\mu\text{g/g}$  [ $n = 5$ ] and 0.5  $\mu\text{g/g}$  [ $n = 4$ ]) in 50% aqueous ethanol or vehicle ( $n = 4$ ) was intraperitoneally administered 5 min before tracer injection (9). The highest concentration of estradiol was chosen on the basis of previous studies in which effective blocking of  $^{18}\text{F}$ -FES was achieved in rats (10). Because of solubility issues, the highest dose of genistein was 5  $\mu\text{g/g}$ , similar to what was previously used in mice (9). Immediately after intravenous administration of  $^{18}\text{F}$ -FHNP, a 60-min emission scan was started and blood samples of 0.1 mL were taken at approximately 10, 20, 30, 40, 50, 60, 90, 120, 150, 180, 300, 450, 600, 750, 900, 1,200, 1,500, 1,800, 2,400, 3,000, and 3,600 s after injection. After collection of each blood sample, 0.1 mL of heparinized saline was injected through the femoral artery to prevent large changes in blood pressure. A 25- $\mu\text{L}$  aliquot of blood was collected from

each sample. The remaining blood was centrifuged (3,461g for 5 min) and a 25- $\mu\text{L}$  aliquot of plasma was collected, whereas the remaining plasma was used for metabolite analysis. Radioactivity levels in the blood and plasma samples were measured with a well counter (LKB Wallac) and used to create the arterial input functions. Immediately after completion of the PET scan, the animals were killed with an excess of isoflurane anesthesia and the bed containing the animal was positioned in a CT scanner (Micro-CT II; CTI, Siemens). A CT image was acquired for 15 min for anatomic localization of the tumor. After the CT scan, the tumors were excised and kept at  $-20^\circ\text{C}$  until further processing for Western blotting. CT imaging and Western blotting were performed as previously described (9).

## Metabolite Analysis

Acetonitrile (50  $\mu\text{L}$ ) was added to approximately 25  $\mu\text{L}$  of plasma sample to

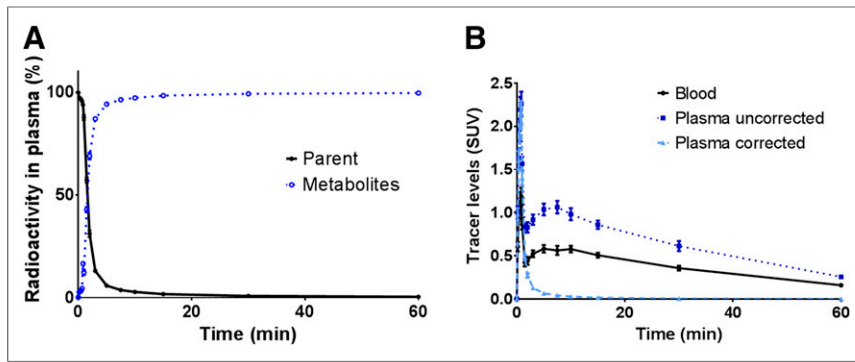


**FIGURE 3.** Metabolism (A) and metabolite-corrected (B) plasma curves for  $^{18}\text{F}$ -FHNP.

precipitate the plasma proteins. The samples were centrifuged at 16,000g for 3 min. A 2- $\mu\text{L}$  aliquot of the supernatant was collected and applied on a thin-layer chromatography plate. The plate was eluted with *n*-hexane/ethyl acetate (1:1) ( $R_f$   $^{18}\text{F}$ -FHNP = 0.7). After elution, radioactivity on the plate was analyzed by phosphor storage imaging. Exposed screens were scanned with a Cyclone phosphor storage system (PerkinElmer), and the percentage of intact  $^{18}\text{F}$ -FHNP as a function of tracer distribution time was calculated by region-of-interest analysis using OptiQuant software (PerkinElmer).

#### Image Reconstruction and Data Analysis

The list-mode data of the emission scans were separated into 21 frames ( $6 \times 10$ ,  $4 \times 30$ ,  $1 \times 120$ ,  $3 \times 150$ ,  $3 \times 300$ , and  $4 \times 600$  s). Emission sinograms were iteratively reconstructed (2-dimensional ordered-subsets expectation maximum, 4 iterations, 16 subsets) after being normalized and corrected for attenuation, scatter, and radioactive decay. The CT and PET images were fused using Inveon Research Workplace software (Siemens Preclinical Solutions), and a volume of interest covering the whole tumor was manually drawn on the CT images and transferred to the corresponding PET images. The last 9 frames of the PET images were summed (10–60 min), and a second volume of interest of the viable part of the tumor was generated automatically with 20% of the maximum tumor uptake as the threshold using a region-growing method. The resulting volumes of interest were used on the original dataset (0–60 min) to generate the corresponding time–activity curves, using standard software (Inveon; Siemens.). Tracer accumulation in tumors is expressed as SUV, which is defined as follows (assuming that all measured tissues have a density of 1 g/mL):

$$\text{SUV} = \frac{\text{tissue activity concentration (MBq/g)} \times \text{body weight (g)}}{\text{injected dose (MBq)}}$$

#### Pharmacokinetic Modeling

**Compartmental Methods.** Since plasma metabolite analysis showed that  $^{18}\text{F}$ -FHNP is rapidly transformed into polar metabolites, it seemed likely that they could contribute to activity in the tumors and thus might introduce a bias in the analysis. Thus, to calculate the pharmacokinetic parameters in this study, 2 model configurations were applied. The first was a 3-tissue-compartment model (3TCM) consisting of an irreversible 2-tissue model for the parent fraction and a reversible 1-tissue model for the metabolite fraction (2 input functions, Fig. 1A). The second configuration was an irreversible 2-tissue-compartment model (2TCM), neglecting the presence of radioactive tissue metabolites (1 input function, Fig. 1B). Pharmacokinetic modeling of tracer kinetics in the tumor was performed using PMOD software (version 3.3). The plasma, blood, and metabolite activity curves were corrected for decay. In the 3TCM, both the metabolite-corrected plasma curve and the metabolite plasma curve were used as the input functions. In the 2TCM, the metabolite-corrected plasma curve was used as the input function. In both models, the whole-blood curve was used for blood volume correction. Blood volume in the tumor was a free modeling parameter. The whole blood, parent  $^{18}\text{F}$ -FHNP, and metabolite input functions were obtained from each animal.

**Graphical Methods.** Graphical analysis methods are simplified linear approximations of compartmental modeling approaches that often can provide more robust estimates of relevant uptake parameters. The dynamic PET data were subjected to Patlak graphical analysis (for irreversible tracer binding), using the metabolite-corrected plasma time–activity curve as the input function (11). This graphical analysis yields slope values equivalent to  $K_i$ , the irreversible uptake rate constant.

**Model Selection.** The model that could best fit tracer kinetics in the tumor was selected on the basis of the Akaike information criterion for small sample sizes and model robustness (12).

**SUV.** To assess whether ER $\beta$  expression could also be estimated from static PET data, the SUV was calculated from the last frame (50–60 min) of the  $^{18}\text{F}$ -FHNP scan.

**Statistical Analysis**

Statistical analyses were performed with Excel 2003 (Microsoft) and Graphpad Prism (version 5.04). Differences between pharmacokinetic models were analyzed using a 2-sided paired Student *t* test. Differences in tracer accumulation between controls and different concentrations of blocker were analyzed using a 2-sided unpaired Student *t* test. Significance was reached when the *P* value was no

**TABLE 1**  
Control Values for  $^{18}\text{F}$ -FHNP Obtained with 2TCM and 3 TCM

Model	2TCM (parent)	3TCM	
		Parent	Metabolite
Blood volume	0.017 $\pm$ 0.008	0.016 $\pm$ 0.069	—
$K_1$ (mL/g/min)	0.022 $\pm$ 0.010	0.0315 $\pm$ 0.020	0.023 $\pm$ 0.043
$k_2$ (1/min)	1.069 $\pm$ 2.619	1.391 $\pm$ 2.527	1.706 $\pm$ 2.711
$k_3$ (1/min)	0.584 $\pm$ 1.105	0.431 $\pm$ 0.493	—
$K_i$ (1/min)	0.010 $\pm$ 0.002	0.0093 $\pm$ 0.002	—
Akaike information criterion	90.3 $\pm$ 15.8	85 $\pm$ 14.6	—

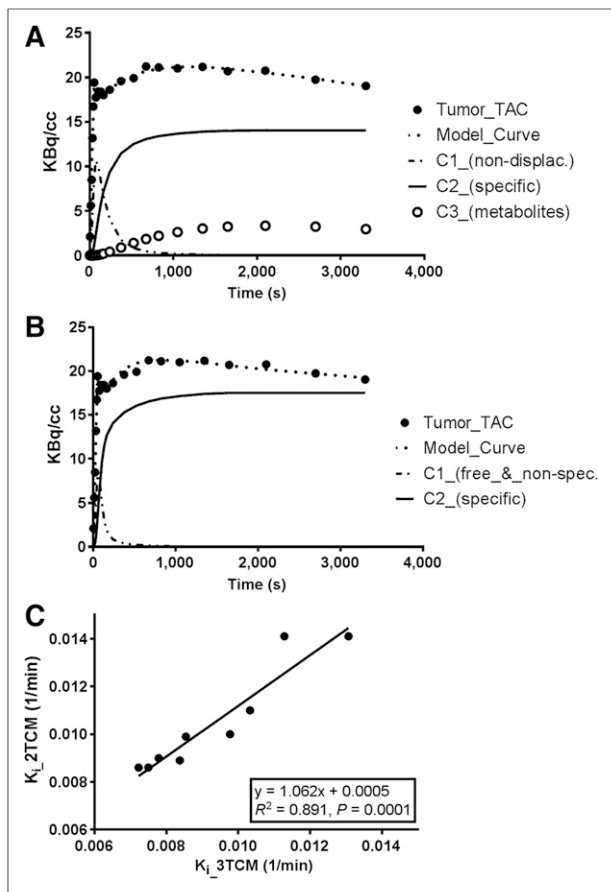


**FIGURE 4.** (A and B) Representative examples of  $^{18}\text{F}$ -FHNP time-activity curves in SKOV3 xenograft and corresponding 3TCM (A) and 2TCM (B) fits, in which C1, C2, and C3 stand for compartments 1, 2, and 3, respectively. (C) Correlation between  $K_i$  values from kinetic analysis using 2TCM and 3TCM.

more than 0.05. Correlations were calculated with the linear regression algorithm in Graphpad Prism (version 5.04) and were considered statistically significant whenever the correlation coefficient ( $r^2$ ) was more than 0.5 and  $P$  was less than 0.05. Throughout the article, values are presented as mean  $\pm$  SEM.

## RESULTS

### PET Images

All rats developed a large SKOV3 xenograft ( $1.87 \pm 0.98 \text{ cm}^3$ ) without estradiol administration. Because of their large size, the tumors became partially necrotic, with  $24\% \pm 19\%$  of the tumor volume being nonviable. Necrotic areas were clearly visible, as  $^{18}\text{F}$ -FHNP scans showed low uptake in the nonviable parts of the tumor (Fig. 2A).

### $^{18}\text{F}$ -FHNP Kinetics in Tumor and Plasma

The kinetics of  $^{18}\text{F}$ -FHNP uptake in SKOV3 xenografts are presented in Figure 2B. Tracer uptake in the tumors reached a maximum within the first minute after tracer injection. This peak uptake was followed by a plateau within 10 min, with no appreciable wash-out within the duration of the scan.

Metabolite analysis revealed that only 6% of the total plasma radioactivity consisted of intact  $^{18}\text{F}$ -FHNP at 5 min after injection, and there was a decrease to only 0.5% at 60 min (Fig. 3A).  $^{18}\text{F}$ -FHNP

kinetics in plasma (metabolite-corrected, Fig. 3B) indicated a rapid monoexponential tracer clearance with a half-life of  $0.29 \pm 0.06 \text{ min}$ .

### Pharmacokinetic Analysis

Both control groups used for the blocking experiments were combined for pharmacokinetic analysis. For initial analysis of the tumor kinetics in control animals ( $n = 9$ ) by compartmental modeling, the reversible and irreversible 2TCM was applied. Both models could be fitted to the data, with no significant difference in the Akaike information criterion values (data not shown). However, when the reversible model was used, most  $k_4$  values were close to zero. Therefore, the irreversible model was then evaluated with either 1 (parent; 2TCM) or 2 (parent and metabolite; 3TCM) input functions. The Akaike information criterion values were  $85 \pm 15$  and  $90 \pm 16$  for the 3TCM and 2TCM, respectively. However, neither model was significantly better than the other ( $P = 0.14$ ). When comparing the individual parameters ( $K_1$ ,  $k_2$ ,  $k_3$ , and  $K_i$ ) obtained from the 2TCM with the corresponding parameters obtained from the 3TCM, we found no significant differences (Table 1). In addition,  $K_i$  values obtained from both models were highly correlated ( $r^2 = 0.89$ ,  $P = 0.0001$ , Fig. 4), as were the  $k_3$  values ( $r^2 = 0.864$ ,  $P = 0.0003$ ) and to a lesser extent the  $K_1$  values ( $r^2 = 0.644$ ,  $P = 0.0092$ ). However, the 3TCM tends to give less robust values, as more variables need to be assessed.

Patlak graphical analysis provided  $K_i$  values (Fig. 5) that correlated strongly with the  $K_i$  obtained from the 2TCM ( $r^2 = 0.93$ ,  $P < 0.0001$ ) and to a lesser extent with  $K_i$  values from the 3TCM ( $r^2 = 0.71$ ,  $P = 0.004$ ). SUV showed reasonably good correlations with  $K_i$  values obtained from the 2TCM ( $r^2 = 0.73$ ,  $P = 0.004$ ), 3TCM ( $r^2 = 0.63$ ,  $P = 0.011$ ), and Patlak analysis ( $r^2 = 0.60$ ,  $P = 0.014$ ) (Supplemental Fig. 1; supplemental materials are available at <http://jnm.snmjournals.org>).

### Correlation of Imaging with ER Expression

Western blotting was performed to quantify the ER $\beta$  and ER $\alpha$  expression in the SKOV3 xenografts (controls,  $n = 9$ ). Immunoreactive bands for ER $\beta$  and ER $\alpha$  were visualized at 55 and 66 kDa, respectively. The ER $\alpha$ / $\beta$ -actin ratio ( $0.17 \pm 0.15$ ) in the tumor was 3 times higher than the ER $\beta$ / $\beta$ -actin ratio ( $0.06 \pm 0.05$ ). As shown in Figure 6, the  $K_i$  of  $^{18}\text{F}$ -FHNP obtained from the 2TCM correlated well with the ER $\beta$ / $\beta$ -actin ratio ( $r^2 = 0.80$ ,  $P = 0.001$ ) but did not correlate with the ER $\alpha$ / $\beta$ -actin ratio.

A similar correlation was obtained when ER $\beta$ / $\beta$ -actin ratios were compared with the  $K_i$  values obtained from Patlak graphical analysis ( $r^2 = 0.68$ ,  $P = 0.006$ ) and with the  $K_i$  values obtained from kinetic analysis using the 3TCM ( $r^2 = 0.72$ ,  $P = 0.004$ ). These findings demonstrated that the  $K_i$  of  $^{18}\text{F}$ -FHNP is a reflection of the ER $\beta$  levels in the tumor. In addition, a moderate correlation between the SUV and the ER $\beta$  levels in the tumor ( $r^2 = 0.47$ ,  $P = 0.04$ ) was found.

### Pharmacokinetic Analysis in the Presence of ER Ligands

In the second phase of the study, the analysis of  $^{18}\text{F}$ -FHNP tumor kinetics using the 2TCM was performed on animals that were administered different concentrations of the ER ligands estradiol (nonspecific) or genistein (ER $\beta$ -selective). As shown in Table 2, a dose-dependent reduction in  $K_i$  in the tumors was observed. The reduction was statistically significant at only the highest dose of estradiol or genistein. A similar competition effect could also be observed when tracer uptake was obtained from a static scan and quantified as SUV (Supplemental Fig. 2).

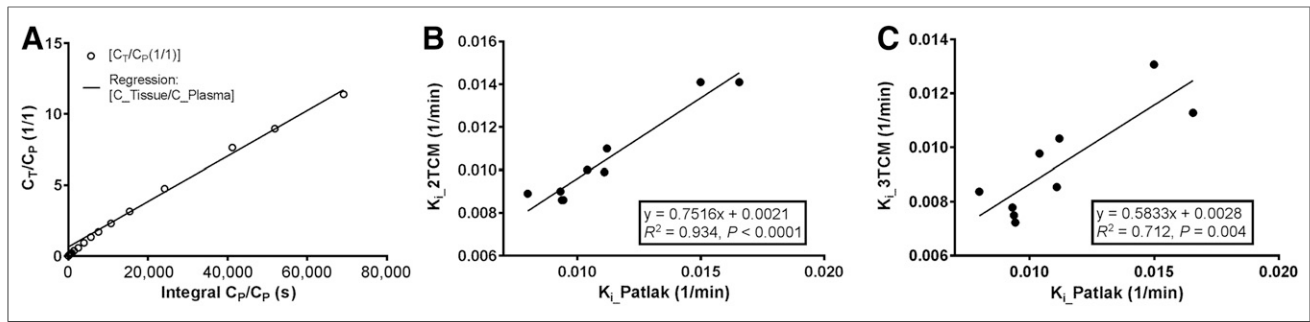


**FIGURE 5.** (A) Representative image of Patlak graphical analysis of  $^{18}\text{F}$ -FHNP uptake in SKOV3 xenograft, in which  $C_T$  and  $C_P$  stand for tissue and plasma compartments, respectively. (B and C) Correlation between Patlak graphical analysis and  $K_i$  values from kinetic analysis using 3TCM (B) or 2TCM (C).

There was a good correlation between the  $K_i$  values and the SUVs ( $n = 32$ ;  $y = 18.46x + 0.073$ ,  $r^2 = 0.69$ ,  $P < 0.0001$ ).

## DISCUSSION

In this study we confirmed that ER $\beta$  expression can be quantified with  $^{18}\text{F}$ -FHNP PET. The imaging parameter that correlated best with ER $\beta$  expression was the influx rate,  $K_i$ . However, SUVs also correlated moderately with ER $\beta$ .

ER $\beta$  has been suggested to be an independent biomarker for benefit from tamoxifen treatment or chemotherapy in patients with ER $\alpha$ -negative breast tumors (3,13). Thus, a proper measurement of ER $\beta$  activity might enable prediction of response to treatment. Unfortunately, immunologic assays (standard method to measure ER levels) of ER $\beta$  by immunohistochemistry can provide information about only a small part of a single lesion. PET imaging, on the other hand, can offer information about the receptor expression in all lesions in the patient. Previously, there have been several attempts to develop a PET tracer for ER $\beta$ , such as 5- $^{18}\text{F}$ -fluoro-(2*R*\*,3*S*\*)-2,3-bis(4-hydroxyphenyl)pentane nitrile, 8 $\beta$ -(2- $^{18}\text{F}$ -fluoroethyl)estradiol, and 7- $^{76}\text{Br}$ -bromo-2-(4-hydroxyphenyl)benzodioxazol-5-ol (14,15). However, these tracers failed to provide evidence of ER $\beta$ -mediated uptake. Recently, we have shown that  $^{18}\text{F}$ -FHNP possesses ER $\beta$  selectivity (9). To our knowledge, the current study was the first in which ER $\beta$  levels were quantified with pharmacokinetic modeling *in vivo* by a noninvasive imaging modality.

Metabolite analysis of plasma showed rapid conversion of  $^{18}\text{F}$ -FHNP into a polar metabolite. Its metabolism rate (6% intact tracer at 5 min) in rats was faster than that of  $^{18}\text{F}$ -FES (50% intact tracer at 6 min) (10). Thus, the fast metabolism of  $^{18}\text{F}$ -FHNP can contribute to its low uptake in the tumors. If  $^{18}\text{F}$ -FHNP possesses affinity toward circulating sex-hormone-binding globulin, the tracer will be protected from degradation in patients and the metabolism rate will likely be slower than in rodents (which lack sex-hormone-binding globulin), as was observed for  $^{18}\text{F}$ -FES (16). Moreover,  $^{18}\text{F}$ -FHNP is rapidly taken up by the tumor (within 1 min), whereas washout of the tracer from the tumor is slow, suggesting irreversible binding. When attempting to fit  $^{18}\text{F}$ -FHNP data to the reversible 2TCM, we obtained very low values of  $k_4$ , confirming that  $^{18}\text{F}$ -FHNP behaves like an irreversible PET tracer. Irreversible tracer binding was also found for other PET tracers for hormone receptor imaging, such as  $^{18}\text{F}$ -fluorodihydrotestosterone (17).

In pharmacokinetic modeling of irreversible tracers, the calculated parameters  $K_1$ ,  $k_2$ ,  $k_3$ , and  $K_i$  are usually obtained from 1- or 2-tissue-compartment analysis, assuming no contribution of metabolites to target tissue activity. These models may be adequately applied in neuroimaging because of the inability of polar metabolites to pass

the blood-brain barrier. However, when tumors are analyzed, metabolites may contribute to tumor activity. Since  $^{18}\text{F}$ -FHNP had a high rate of metabolism, evaluation of the contribution of metabolites to uptake in the tumor was crucial. Therefore, we tested a 3TCM that takes the presence of metabolites into account. As depicted in Figure 4, the contribution of the metabolites to the total activity in the tumor was low ( $12\% \pm 5\%$ ). When comparing the 3TCM with the 2 TCM, we found a good correlation between the two methods for both  $k_3$  and  $K_i$ . This suggests that, despite the high amount of metabolites in circulation, uptake and trapping in the tumor are mainly due to the intact tracer. This possibility is in agreement with observations for other hormone receptor tracers that were rapidly converted into polar metabolites (mainly sulphates and glucuronides). These metabolites are polar, resulting in limited access into intracellular space, and therefore they do not significantly bind to the intracellular ER (17,18).

Graphical analysis gave results similar to compartmental modeling, as the  $K_i$  values obtained from the Patlak analysis correlated strongly with the  $K_i$  values obtained in the 2TCM. Irrespective of whether compartmental modeling or graphical analysis is applied for the analysis, however, arterial blood sampling and metabolite analysis are recommended to obtain the  $K_i$  values. However, this recommendation may hamper clinical applicability. To avoid blood sampling, an input function could be extracted noninvasively from the blood pools of the PET dynamic images or by scaling an arterial blood population input function using a venous blood sample. However, these alternative methods would require validation. Thus, in this study, to further simplify data acquisition and analysis procedures, tracer uptake, expressed as SUV, obtained from a static scan without blood sampling was evaluated as a potential parameter to describe ER $\beta$  expression. The SUV correlated well with  $K_i$  values obtained from kinetic analysis using the 2TCM. Simplified methods such as SUV do not take into account a possible influence of metabolite formation and blood volume, possibly explaining why  $K_i$  correlated better with ER $\beta$  expression than did SUV. Nevertheless, our study also found that SUV correlated moderately with ER $\beta$  expression in the tumors. It is important to emphasize that  $K_i$  and SUVs correlated with only ER $\beta$  expression in the tumors and not with ER $\alpha$  expression, confirming the selectivity of  $^{18}\text{F}$ -FHNP for ER $\beta$ .

$^{18}\text{F}$ -FHNP metabolism and kinetics in blood and plasma were not affected by the presence of different concentrations of the ER ligands estradiol and genistein, suggesting that metabolism and clearance pathways were not saturated by the competitors. When  $^{18}\text{F}$ -FHNP was given with different concentrations of estradiol or genistein, a dose-dependent reduction in tracer uptake in the viable part of the tumor was observed. The  $K_i$  and SUVs correlated well for

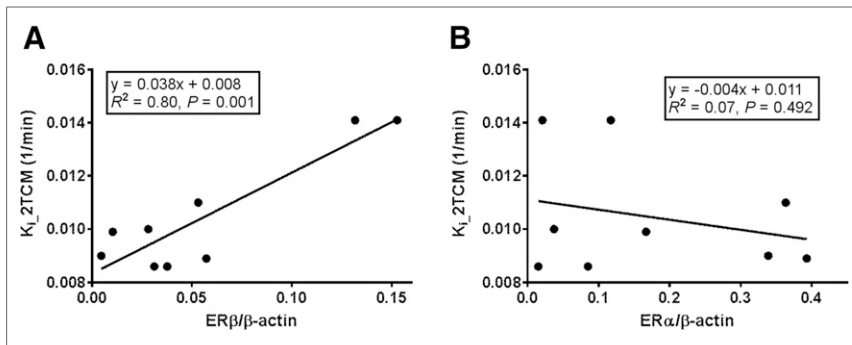


**FIGURE 6.** Correlation of  $K_i$  values obtained from kinetic analysis using 2 TCM ( $n = 9$ ) with ER $\beta$  (A) and ER $\alpha$  (B) density obtained from Western blotting assay.

the different concentrations of ER ligands, indicating that changes in  $^{18}\text{F}$ -FHNP kinetics could be observed with both metrics, and suggesting the possibility of using a simplified imaging protocol to estimate receptor availability that does not involve blood sampling.

Uptake of  $^{18}\text{F}$ -FHNP is only 30% inhibited by estradiol or genistein. This low inhibition percentage most likely is related to the relatively low amount of ER $\beta$  expression in these tumors. Low receptor expression yields only a low absolute amount of specific tracer binding. In contrast, nonspecific binding is independent of receptor expression; as a consequence, the percentage of specific binding relative to the amount of nonspecific binding will be low. Therefore, it would be advisable to perform further studies in a more suitable model with tumors that display higher ER $\beta$  expression levels. Moreover, one cannot exclude the possibility that the amounts of agonists used in these experiments were too low to completely saturate all receptors. Thus, higher concentrations of genistein and estradiol should also be tested in future studies.

## CONCLUSION

In this study, we were able to prove that  $^{18}\text{F}$ -FHNP trapping in the tumor correlates with ER $\beta$  expression but not with ER $\alpha$ , thus confirming the subtype selectivity of this PET tracer. The most suitable parameter to describe ER $\beta$  expression with  $^{18}\text{F}$ -FHNP PET is the

**TABLE 2**

Comparison of SUVs Obtained from PET Data 50–60 Minutes After Injection of  $^{18}\text{F}$ -FHNP and  $K_i$  Values Obtained from 2TCM Fit for All Groups

Parameter	SUV	$K_i$ (1/min)
<b>Estradiol</b>		
Control ( $n = 9$ )	0.28 ± 0.04	0.0105 ± 0.0020
0.003 $\mu\text{g/g}$ ( $n = 4$ )	0.26 ± 0.05	0.0105 ± 0.0034
0.03 $\mu\text{g/g}$ ( $n = 5$ )	0.25 ± 0.06	0.0100 ± 0.0030
0.3 $\mu\text{g/g}$ ( $n = 5$ )	0.18 ± 0.05*	0.0073 ± 0.0020*
<b>Genistein</b>		
Control ( $n = 9$ )	0.28 ± 0.04	0.0105 ± 0.0020
0.5 $\mu\text{g/g}$ ( $n = 5$ )	0.25 ± 0.01	0.0082 ± 0.0014
5 $\mu\text{g/g}$ ( $n = 4$ )	0.21 ± 0.03*	0.0076 ± 0.0011*

\* $P < 0.05$  when compared with controls.

influx rate constant,  $K_i$ , when a dynamic PET acquisition protocol with arterial blood sampling and metabolite analysis is applied. However, simplification of the acquisition and analysis protocol is possible, as SUV could also be applied to assess ER $\beta$  levels.

## DISCLOSURE

This study was part of the MAMMOTH project, funded by the Center for Translational Molecular Medicine (CTMM) in The Netherlands. No other potential conflict of interest relevant to this article was reported.

## REFERENCES

- Minutolo F, Macchia M, Katzenellenbogen BS, Katzenellenbogen JA. Estrogen receptor  $\beta$  ligands: recent advances and biomedical applications. *Med Res Rev*. 2011;31:364–442.
- Fox EM, Davis RJ, Shupnik MA. ER $\beta$  in breast cancer: onlooker, passive player, or active protector? *Steroids*. 2008;73:1039–1051.
- Yan Y, Li X, Blanchard A, et al. Expression of both estrogen receptor-beta 1 (ER- $\beta$ ) and its co-regulator steroid receptor RNA activator protein (SRAP) are predictive for benefit from tamoxifen therapy in patients with estrogen receptor-alpha (ER- $\alpha$ )-negative early breast cancer (EBC). *Ann Oncol*. 2013;24:1986–1993.
- Marcom PK, Isaacs C, Harris L, et al. The combination of letrozole and trastuzumab as first or second-line biological therapy produces durable responses in a subset of HER2 positive and ER positive advanced breast cancers. *Breast Cancer Res Treat*. 2007;102:43–49.
- Smith IE, Walsh G, Skene A, et al. A phase II placebo-controlled trial of neoadjuvant anastrozole alone or with gefitinib in early breast cancer. *J Clin Oncol*. 2007;25:3816–3822.
- van Kruchten M, Glaudemans AWJM, de Vries EFJ, et al. PET imaging of estrogen receptors as a diagnostic tool for breast cancer patients presenting with a clinical dilemma. *J Nucl Med*. 2012;53:182–190.
- Niikawa H, Suzuki T, Miki Y, et al. Intratumoral estrogens and estrogen receptors in human non-small cell lung carcinoma. *Clin Cancer Res*. 2008;14:4417–4426.
- Ikeda K, Shiraishi K, Yoshida A, et al. Synchronous multiple lung adenocarcinomas: estrogen concentration in peripheral lung. *PLoS One*. 2016;11:e0160910.
- Antunes IF, van Waarde A, Dierckx RA, de Vries EGE, Hospers GAP, de Vries EF. Synthesis and evaluation of the new estrogen receptor  $\beta$  selective radioligand [ $^{18}\text{F}$ ]FHNP: comparison with [ $^{18}\text{F}$ ]FES. *J Nucl Med*. 2017;58:554–559.
- Khayum MA, de Vries EFJ, Glaudemans AWJM, Dierckx RAJO, Doorduyn J. In vivo imaging of brain estrogen receptors in rats: a 16 $\alpha$ - $^{18}\text{F}$ -fluoro-17 $\beta$ -estradiol PET study. *J Nucl Med*. 2014;55:481–487.
- Patlak CS, Blasberg RG, Fenstermacher JD. Graphical evaluation of blood-to-brain transfer constants from multiple-time uptake data. *J Cereb Blood Flow Metab*. 1983;3:1–7.
- Glattig G, Kletting P, Reske SN, Hohl K, Ring C. Choosing the optimal fit function: comparison of the Akaike information criterion and the F-test. *Med Phys*. 2007;34:4285–4292.
- Elebro K, Borgquist S, Rosendahl AH, et al. High estrogen receptor  $\beta$  expression is prognostic among adjuvant chemotherapy-treated patients: results from a population-based breast cancer cohort. *Clin Cancer Res*. 2017;23:766–777.
- Yoo J, Dence CS, Sharp TL, Katzenellenbogen JA, Welch MJ. Synthesis of an estrogen receptor  $\beta$ -selective radioligand: 5-[ $^{18}\text{F}$ ]fluoro-(2R\*,3S\*)-2,3-bis(4-hydroxyphenyl)pentanenitrile and comparison of in vivo distribution with 16 $\alpha$ -[ $^{18}\text{F}$ ]fluoro-17 $\beta$ -estradiol. *J Med Chem*. 2005;48:6366–6378.
- Lee JH, Peters O, Lehmann L, et al. Synthesis and biological evaluation of two agents for imaging estrogen receptor  $\beta$  by positron emission tomography: challenges in PET imaging of a low abundance target. *Nucl Med Biol*. 2012;39:1105–1116.
- Tewson TJ, Mankoff DA, Peterson LM, Woo I, Petra P. Interactions of 16 $\alpha$ -[ $^{18}\text{F}$ ]fluoroestradiol (FES) with sex steroid binding protein (SBP). *Nucl Med Biol*. 1999;26:905–913.
- Beattie BJ, Smith-Jones PM, Jhanwar YS, et al. Pharmacokinetic assessment of the uptake of 16 $\beta$ - $^{18}\text{F}$ -fluoro-5 $\alpha$ -dihydrotestosterone (FDHT) in prostate tumors as measured by PET. *J Nucl Med*. 2010;51:183–192.
- Mankoff DA, Tewson TJ, Eary JF. Analysis of blood clearance and labeled metabolites for the estrogen receptor tracer [ $^{18}\text{F}$ ]-16 alpha-fluoroestradiol (FES). *Nucl Med Biol*. 1997;24:341–348.